Hindawi
Wireless Communications and Mobile Computing
Volume 2018, Article ID 8509693, 16 pages
https://doi.org/10.1155/2018/8509693

Research Article

Performance Analysis of RF-Powered Cognitive Radio Networks with Integrated Ambient Backscatter Communications

Longteng Xu,[1] **Kun Zhu**,[1] **Ran Wang**,[1] **and Shimin Gong**[2]

[1]*Nanjing University of Aeronautics and Astronautics, Nanjing, China*
[2]*Shenzhen Institutes of Advanced Technology, Shenzhen, China*

Correspondence should be addressed to Kun Zhu; zhukun@nuaa.edu.cn

Received 24 November 2017; Accepted 11 February 2018; Published 2 April 2018

Academic Editor: Hina Tabassum

Integrating ambient backscatter communications into RF-powered cognitive radio networks has been shown to be a promising method for achieving energy and spectrum efficient communications, which is very attractive for low-power or no-power communications. In such scenarios, a secondary user (SU) can operate in either transmission mode or backscatter mode. Specifically, an SU can directly transmit data if sufficient energy has been harvested (i.e., transmission mode). Or an SU can backscatter ambient signals to transmit data (i.e., backscatter mode). In this paper, we investigate the performance of such systems. Specifically, channel inversion power control and an energy store-and-reuse mechanism for secondary users are adopted for efficient use of harvested energy. We apply stochastic geometry to analyze coverage probability and achievable rates for both primary and secondary users considering both communication modes. Analytical tractable expressions are obtained. Extensive simulations are performed and the numerical results show the validity of our analysis. Furthermore, the results indicate that the performance of secondary systems can be improved with the integration of both communication modes with only limited impact on the performance of primary systems.

1. Introduction

In recent years, the demand for smart systems (e.g., on-body sensing for e-Healthy) is growing fast. For such systems, the deployed sensors usually need to work continuously and transmit collected data for upper layer applications. Since most sensors have limited battery and limited spectrum resources, energy-efficient and spectrum efficient wireless communications are required.

Several techniques have been developed for achieving low-power or even no-power communications in a spectrum efficient manner, among which ambient backscatter communications and radio-frequency (RF) powered cognitive communications are two remarkable ones. In [1], authors investigate practical backscatter for on-body sensors by using the signals from Wi-Fi or Bluetooth. Such a backscatter system based on Wi-Fi is referred to as Wi-Fi backscatter [2]. Be different from RF identification (RFID) which needs a dedicated signal emitter (RFID reader) [3], Wi-Fi backscatter does not need dedicated reader. However, it does not perform well in outdoor environment. While ambient backscatter communication [4] is also a type of passive communication which utilizes ambient RF signals (e.g., TV signals) to transmit data, no dedicated signal source is required, which makes no-power wireless communications possible. However, the communications are vulnerable since backscattered signals are usually weak and volatile.

Another technique, harvesting energy from ambient RF signals, has been proposed to support energy-efficient communications [5–7]. Besides, RF-powered cognitive radio network (CRN) offers a method to utilize primary transmitter (PTs) signals as the energy source for secondary transmitters (STs). A main problem is that the transmission opportunities of RF-powered STs are limited by the harvested energy and channel availability.

In this work, we consider the integration of ambient backscatter communications into RF-powered cognitive radio networks in a similar way to [8]. In this case, these two techniques could complement each other to jointly achieve the

advantages while overcoming the individual shortcomings. Specifically, in such scenarios, the secondary transmitters can operate in two modes, that is, transmission mode and backscatter mode. In transmission mode, an ST can directly transmit data to its receiver if sufficient energy has been harvested and the channel is available. When the channel is busy, an ST can switch to backscatter mode which backscatters the ambient signals to transmit its own data.

In other words, in our cognitive radio network, the transmission of secondary transmitters falls into interweave paradigm to utilize white spaces of specific channels [9], and the needed energy is harvested from existing signals. As for backscatter communication, in some extent it falls into overlay paradigm since the backscattered signals from secondary transmitters to primary receivers can be ignored which will be stated in more detail in the following [9–11]. As for the primary user activity model, which has a vital influence on cognitive users' performance, that is, directly determining spectrum access time of cognitive users, in this paper follows a simplified ON/OFF model [12] wherein total active (ON) duration and inactive (OFF) duration of a primary user are fixed. Besides, the details of spectrum sensing are omitted in this paper. Other complex and widely used primary user activity models and spectrum analysis can be found in [12–15].

Note that several existing works have been done for the integration of backscatter communications with cognitive radio networks or cellular networks. In [16], authors give an overview of backscatter assisted wireless powered communications and introduce a multiple access scheme in cognitive radio networks. The tradeoff analysis in RF-powered backscatter CRNs is provided in [17]. However, only one single cell is considered and no performance analysis is provided. In [18], the integration of backscatter communications with heterogeneous cellular networks is proposed and analyzed. In [19], a backscatter network is analyzed by using stochastic geometry, but dedicated power beacons are deployed to support the communication, while, in [20, 21], a single hybrid transmitter harvests energy from multiple ambient transmitters, transmits its own signal, or backscatters existing signals to a hybrid receiver, and its performance is analyzed.

In this paper, we investigate the performance of ambient backscatter communications in RF-powered cognitive radio network. Specifically, we propose an analytical framework based on stochastic geometry [22–24], with which the tractable expressions for coverage probability and achievable rates for both primary and secondary users considering both communication modes are obtained. We perform extensive simulations and the numerical results demonstrate the validity of the theoretical analysis. Also, the results indicate that secondary systems can achieve improved performance while having only limited impact on the primary systems, which show the effectiveness of integration.

The rest of the paper is organized as follows: Section 2 presents the comprehensive system model. Section 3 presents channel inversion power control and energy storage and reusing. Analytical expressions are given in Section 4. In Section 5, numerical results from analysis and simulations are described. Finally, Section 6 draws the conclusions.

2. System Model

2.1. Network Model. We consider a cognitive cellular network in which macro base stations (MBSs, i.e., PTs, Y) serve primary cellular users (PRs, U) in the downlink while overlaid by cognitive secondary users. Each PR will connect to the nearest MBS. Besides, there are secondary transmitters (STs, X) equipped with energy storage and secondary receivers (SRs, Z). An ST can communicate with an SR by either backscattering signals or emitting its own signals. Since backscattered signal is weak, the distance from backscattering node (i.e., ST) to receiving node (i.e., SR) is limited. It is shown in [4] that, for achieving 1 kbps information rate in outdoor environment, 2.5 feet is the maximum distance. Therefore, in this paper, for ease of analysis, we assume that an SR is at a constant small distance d to its associated ST in an isotropic direction [19].

MBSs and PRs are modeled by homogeneous Poisson point processes (HPPP) Φ and $\widetilde{\Phi}_U$ with intensities λ and $\widetilde{\lambda}_U$, respectively. STs are uniformly distributed in annular regions with radii R_m and R_M centered at each MBS. Each ST can be loosely seen as a result of random and independent displacement of the MBS. In each annular region, the number of STs is $N_{\mathrm{ST}} \sim \pi(\Lambda)$, where $\pi(\Lambda)$ is the Poisson distribution with parameter Λ. The distribution model of STs then is similar to a Matern cluster process where Φ is the parent process [25]. An inner radius $R_m > 0$ of the annular region is considered for avoiding singularity of integral in the derivation process and the outer radius R_M is related to *circuit power constraint* described in the following part.

We assume each PR is associated with its nearest MBS. The probability density function (pdf) of distance r from a PR to its nearest MBS is [23]

$$f(r) = 2\pi\lambda r e^{-\pi\lambda r^2}. \tag{1}$$

If a point is uniformly distributed within a circle with radius R and r is the distance to the center, the pdf of r is $f_o(r) = 2r/R^2$ [26]. By using conditional probability, we can get the pdf of distance r from an ST to its MBS as

$$\begin{aligned} F\left(R \mid r \geq R_m\right) &= \frac{P\left(R_m \leq r \leq R\right)}{P\left(r \geq R_m\right)} = \frac{R^2 - R_m^2}{R_M^2 - R_m^2}, \\ f_{\geq R_m}(r) &\triangleq f\left(r \mid r \geq R_m\right) = \frac{\mathrm{d}F\left(R \mid r \geq R_m^2\right)}{\mathrm{d}r} \\ &= \frac{2r}{R_M^2 - R_m^2}. \end{aligned} \tag{2}$$

Without loss of generality, according to Slivnyak's theorem [27], we analyze a typical PR (U_0) and a typical SR (Z_0) located at the origin. The typical SR's corresponding ST and MBS are also similarly typical ST (X_0) and typical MBS (Y_0), respectively. Figure 1 illustrates randomly generated positions of MBSs, PRs, and STs. Figure 2 shows the system model.

2.2. Channel Model. All MBSs share the same available channel set $\mathbf{C} = \{c_1, c_2, \ldots, c_{|\mathbf{C}|}\}$, where $|\mathbf{C}| = N_{\mathrm{ch}}$ is the number of channels. We assume $\widetilde{\lambda}_U \gg \lambda$ and there is one and only

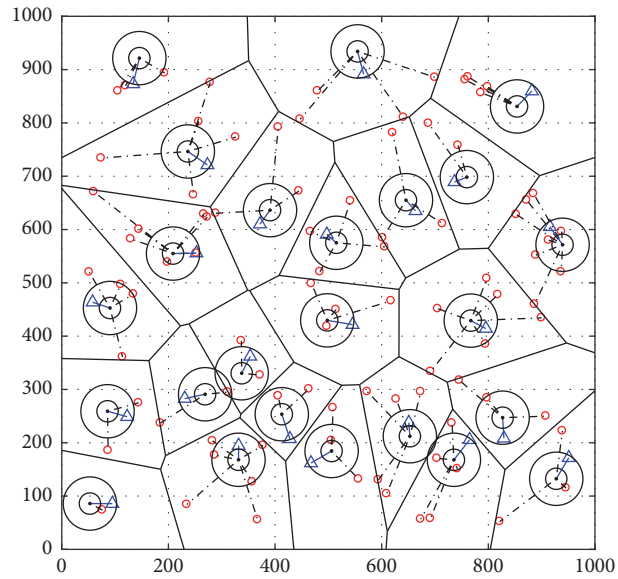

FIGURE 1: Network composition illustration. Centers of dual-circles (annular regions), red dots, and blue triangles represent MBSs, primary receivers, and secondary transmitters, respectively. To ensure visibility, only one ST is showed in an annular region and all SRs are omitted. (Radii of annular regions in the illustration are enlarged.)

one active PR in each channel of a cell, so active PRs in a generic channel form an HPPP Φ_U with intensity $\lambda_U = \lambda$ by independent thinning.

We also assume that STs in each cell have equal probabilities to access a channel when it is idle, and no two STs share the same channel. However, STs in different cells may not have equal probabilities since numbers of STs in different cells may differ from each other. This means the thinned processes are not HPPPs. But for ease of analysis, in this paper, similar to the assumptions in [6, 28–30], we assume STs in different cells in a generic channel constitute an HPPP by random displacement and thinning.

Besides, if there are N_{ST} STs in one annular region, the probability that a channel in $\mathbf{C}$ is used by an ST is $N_{\mathrm{ST}}/N_{\mathrm{ch}}$, while if $N_{\mathrm{ST}} > N_{\mathrm{ch}}$, the probability is 1. Since $N_{\mathrm{ST}} \sim \pi(\Lambda)$, the probability that a channel is used averaged over N_{ST} is

$$p_{\mathrm{ch}} = \sum_{k=0}^{N_{\mathrm{ch}}} \mathbb{P}\left[N_{\mathrm{ST}} = k\right] \frac{k}{N_{\mathrm{ch}}} + \sum_{k=N_{\mathrm{ch}}+1}^{\infty} \mathbb{P}\left[N_{\mathrm{ST}} = k\right] \cdot 1 = 1 + \frac{(\Lambda - N_{\mathrm{ch}})\,\Gamma(N_{\mathrm{ch}}, \Lambda) - e^{-\Lambda}\Lambda^{N_{\mathrm{ch}}}}{\Gamma(1 + N_{\mathrm{ch}})}, \tag{3}$$

where $\Gamma(z) = \int_0^{\infty} t^{z-1}e^{-t}\mathrm{d}t$ is the Gamma function and $\Gamma(z,a) = \int_a^{\infty} t^{z-1}e^{-t}\mathrm{d}t$ is the upper incomplete Gamma function. So STs in a generic channel form an HPPP Φ_{ST} with intensity $\lambda_{\mathrm{ST}} = p_{\mathrm{ch}}\lambda$ by independent thinning and random displacement. And p_{ch} is termed *channel in use probability*.

An extreme case is that Λ is high enough and $p_{\mathrm{ch}} = 1$ holds. This equals the setting that only one channel is considered in the network and channels of all cells are used. In this case, besides p_{ch}, other details of the network remain unchanged, so does the analysis.

We assume that each channel experiences a constant noise power W and exponential path-loss $\ell(r) = r^{-\alpha}$ (or $\ell(X-Y) = \|X-Y\|^{-\alpha}$) with a uniform exponent $\alpha > 2$, where r is a distance, $X, Y \in \mathbb{R}$ are two points, and $\|\cdot\|$ is the Euclidean norm. Independent Rayleigh fading is considered which remains constant within one time slot. The fading from a PR/ST to its corresponding MBS is $h \sim \exp(\mu_h)$, fading from an ST to its SR is $q \sim \exp(\mu_q)$, and interference fading from an MBS/PR/ST to a PR/SR is $g \sim \exp(\mu_g)$. Moreover, for convenience we set a time slot duration to be a unit time.

2.3. Communication Model. When an MBS serves a PR, it may turn into busy or idle mode during each time slot. We further divide each time slot into M minislots [19] and all minislots are synchronized among MBSs. In addition, we assume that each MBS randomly and independently turns into idle mode in one of the minislots. With such assumptions, when the MBS is transmitting, we consider that an ST performs energy harvesting (EH) and ambient backscatter communication (BC) in D_E and D_B minislots, respectively, and we have $D_E + D_B + 1 = M$. Minislots for EH and BC of each ST are also randomly and independently selected with equal probability. Besides, the ST performs traditional information transmission (IT) using the harvested energy when the MBS is idle. In the following, these two communication modes are termed BC mode and IT mode, respectively. An example of minislots assignment and selection when $M = 7$ is given in Figure 3.

In a generic minislot, STs performing energy harvesting form an HPPP Φ_{eh} with intensity $\lambda_{\mathrm{eh}} = (D_E/M)\lambda_{\mathrm{ST}}$, which can be seen as the thinning of Φ_{ST} since each ST may work in EH mode within a minislot with probability D_E/M. Similarly, STs in BC mode and IT mode form HPPPs Φ_{bc} and $\widetilde{\Phi}_{\mathrm{it}}$ with intensities $\lambda_{\mathrm{bc}} = (D_B/M)\lambda_{\mathrm{ST}}$ and $\widetilde{\lambda}_{\mathrm{it}} = \lambda_{\mathrm{ST}}/M$, respectively. Moreover, MBSs in busy mode also form an HPPP Φ_{bs} with intensity $\lambda_{\mathrm{bs}} = (1 - 1/M)\lambda$.

We further assume that the SR knows about its ST's work mode so as to perform corresponding decoding. Saturation condition is also assumed where a data packet is always ready for transmission.

Besides, we assume that when an ST performs BC, a portion β of the received power is used for BC, and the backscatter efficiency is η_b. So the backscatter power of a generic ST is

$$P_{\mathrm{bc}} = \beta\eta_b \|X - Y\|^{-\alpha} h, \tag{4}$$

where $\|X - Y\|$ is the distance from the MBS to the ST, while the remaining portion $1-\beta$ is stored as energy [19] along with received power in EH mode. And the conversion efficiency is η. In this case, the harvested energy within a time slot is

$$E_H = \eta\left(\frac{D_E}{M} + (1-\beta)\frac{D_B}{M}\right) r^{-\alpha} h = \frac{D_{\mathrm{eb}} h}{M r^{\alpha}}, \tag{5}$$

where $D_{\mathrm{eb}} = \eta(D_E + (1-\beta)D_B)$.

In order to perform IT, an ST must satisfy the circuit power constraint that E_H is more than that consumed E_C by

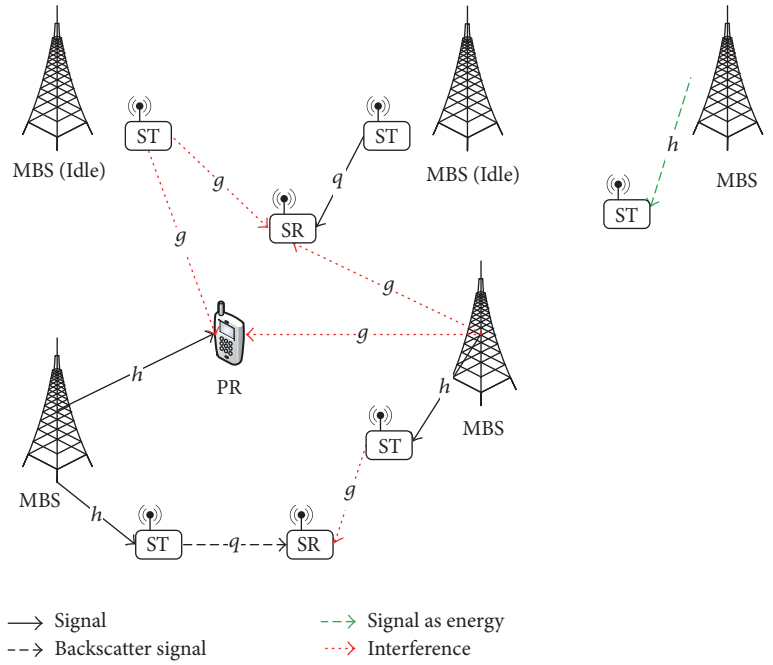

Figure 2: System model of our network. h, g, q refer to three types of fading described in Section 2.2.

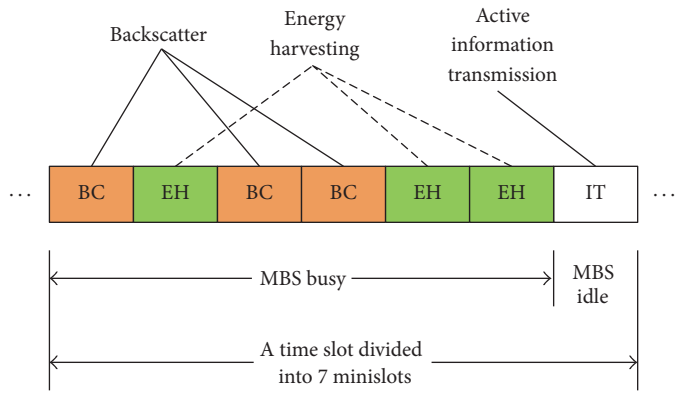

Figure 3: An example of minislots assignment and selection for different mode when number of minislots is 7.

the circuit, while the remaining power $E_H - E_C$ is used for data transmission. Since a time slot lasts a unit time, we will also describe E_H and E_C as the power. The average harvested energy can be obtained as

$$\mathbf{E}_h\left[E_H\right] = \int_0^\infty \mu_h e^{-\mu_h h} \frac{D_{\text{eb}} h}{M r^\alpha} \mathrm{d}h = \frac{D_{\text{eb}}}{\mu_h M r^\alpha}, \tag{6}$$

and the limitation of distance r from an ST to an MBS, that is, R_M, can be derived as

$$\mathbf{E}_h\left[E_H\right] - E_C > 0 \Longleftrightarrow r < R_M \triangleq \left(\frac{D_{\text{eb}}}{\mu_h M E_C}\right)^{1/\alpha}, \tag{7}$$

where R_M is based on the setting that STs distributed in the annular region should satisfy the circuit power constraint. When fading is considered, the probability that harvested energy E_H is above demand is

$$\begin{aligned} G(x) &\triangleq \mathbb{P}\left[E_H > x\right] = \mathbb{P}\left[\frac{D_{\text{eb}} h}{M r^\alpha} > x\right] \\ &= \int_{R_m}^{R_M} \int_{M r^\alpha x / D_{\text{eb}}}^{\infty} f_{\geq R_m}(r) \cdot f(h)\, \mathrm{d}h\, \mathrm{d}r \\ &= \frac{2\left(H(x, R_m) - H(x, R_M)\right)}{\alpha\left(R_M^2 - R_m^2\right)}, \end{aligned} \tag{8}$$

where x is a parameter representing energy demand, r is the distance from an ST to its MBS, $f_{\geq R_m}(r)$ is the pdf given in (2), h is the fading, and

$$H(x,y) = y^2 E\left(\frac{\alpha-2}{\alpha}, J(x)\, y^{\alpha}\right),$$
$$J(x) = \frac{x\mu_h M}{D_{\text{eb}}}, \tag{9}$$
$$E(n,z) = \int_1^{\infty} e^{-zt} t^{-n} \mathrm{d}t \ \ (\text{exponential integral}),$$

where α, μ_h, M, and D_{eb} have been presented. Therefore, the constraint satisfaction probability p_{sat} of an ST is

$$p_{\text{sat}} \triangleq \mathbb{P}\left[E_H - E_C > 0\right] = G\left(E_C\right). \tag{10}$$

In the following, p_{sat} will also be termed *power satisfaction probability*. Taking this probability into account, STs in IT mode that have enough energy form an HPPP Φ_{it} with intensity $\lambda_{\text{it}} = p_{\text{sat}}\widetilde{\lambda}_{\text{it}} = p_{\text{sat}}\lambda_{\text{ST}}/M$. In the following, these STs are called *working STs*.

When performing IT, the available energy is $E_H - E_C$, but for ease of analysis, in this paper we adopt the setting that a portion ξ of the harvested energy E_H can be used for active information transmission [31] and energy not used is ignored in different time slots. So the transmit power of a generic ST is

$$P_{\text{it}} = \frac{\xi E_H}{1/M} = \xi D_{\text{eb}} \left\|X - Y\right\|^{-\alpha} h, \tag{11}$$

where $\|X - Y\|$ is the distance from the MBS to the ST.

2.4. Interference Model. In [32], authors mentioned *interference regeneration* that a backscatter node reflects all incident signals which leads to a square number of interference components for each SR. One effective solution is to adopt spread spectrum techniques. In this paper, we simplify this problem and assume that an ST backscatters only the signal from its corresponding MBS.

2.4.1. Backscattered Signal to an SR in IT Mode. Backscattered signal from an ST to an SR in IT mode is considered as an extra path. We assume an SR in IT mode has the ability to eliminate multipath effect like PRs [4], so such interference is ignored.

2.4.2. Transmitted Signal to an SR in BC Mode. Since an SR in BC mode senses and decodes backscattered signal by sensing changes in the signal caused by backscattering [4], we also ignore such interference.

2.4.3. Backscattered Interference to an SR in BC Mode. Such interference comes from other STs (X_i) in BC mode whose corresponding MBSs (Y_i) are in busy mode. Interfering STs come from $\Phi_{\text{bc}} \setminus \{X_0\}$. Such interference is firstly transmitted from an MBS to its ST, encountering path-loss $\ell(X_i - Y_i)$ and Rayleigh fading $h \sim \exp(\mu_h)$, then it is backscattered from an ST to the typical SR, encountering path-loss $\ell(X_i - Z_0)$ and Rayleigh fading $g \sim \exp(\mu_g)$. The interference is denoted as

$$I_{\text{bc}} = \sum_{X_i \in \Phi_{\text{bc}} \setminus \{X_0\}} P_{\text{bc}_i} \left\|X_i - Z_0\right\|^{-\alpha} g_i, \tag{12}$$

where P_{bc_i} is the backscatter power of an ST in BC mode given in (4).

2.4.4. Transmitted Interference to an SR in IT Mode. Such interference comes from other MBSs in busy mode and other STs in IT mode whose corresponding MBSs are in idle mode. Interfering MBSs come from $\Phi_{\text{bs}} \setminus \{Y_0\}$. Such interference is transmitted from an MBS to the typical SR, encountering path-loss $\ell(Y_i - Z_0)$ and Rayleigh fading $g \sim \exp(\mu_g)$. Interfering STs come from $\Phi_{\text{it}} \setminus \{X_0\}$. Such interference is firstly transmitted from an MBS to its ST, encountering path-loss $\ell(X_i - Y_i)$ and Rayleigh fading $h \sim \exp(\mu_h)$, then it is backscattered from the ST to the SR, encountering path-loss $\ell(X_i - Z_0)$ and Rayleigh fading $g \sim \exp(\mu_g)$. The interference is denoted as

$$\begin{aligned} I_{\text{sum}} &= I_{\text{it}} + I_{\text{bs}} \\ &= \sum_{X_i \in \Phi_{\text{it}} \setminus \{X_0\}} P_{\text{it}_i} \left\|X_i - Z_0\right\|^{-\alpha} g_i \\ &\quad + \sum_{Y_i \in \Phi_{\text{bs}} \setminus \{Y_0\}} \left\|Y_i - Z_0\right\|^{-\alpha} g_i, \end{aligned} \tag{13}$$

where I_{it}, I_{bs} represent two interference components, respectively, and P_{it_i} is the transmit power of an ST in IT mode given in (11).

2.4.5. Transmitted Interference to a PR. All interference to a PR is identical to the interference to an SR in IT mode. We will analyze performance of a PR located at the origin encountering no interference from STs to make a comparison to reveal the effect on PRs.

2.5. Rate Model for Backscatter Link. In [4], the bit rate (alternating sequence of ones and zeros) of the ambient backscatter prototype is related to the setting of circuit elements. Similar settings are also used in [8, 17, 18] and will be used in this paper, too. Besides, we assume if the signal-to-interference-plus-noise-ratio (SINR) of backscatter communication is above a threshold, the predesigned rate can be achieved [20].

Notations used in this paper are listed in the Notations.

3. Channel Inversion Power Control and Energy Storage and Reusing

Since energy is precious for secondary users, the harvested energy should be used more efficiently. So in this section we apply channel inversion power control to ST's active information transmission to avoid poor signal transmitted from STs. Moreover, since power control is applied, there is a higher probability that secondary users do not use up its energy. Therefore, we also propose a simple energy storage and reusing mechanism, to improve the utilization of harvested energy.

3.1. Channel Inversion Power Control. In this part, we use channel inversion power control to let STs make less interference to primary users and conserve energy, while keeping

their active transmission reliable. To be specific, an ST in IT mode will not use up its energy but transmit at a power to invert the path-loss to make sure that the average received power at its SR is equal to an SR's sensitivity ρ in IT mode [33]. Specifically, if the available energy is enough to support channel inversion power control, the ST will transmit at power ρd^{α}, where d is the distance between a secondary pair. So ρ will highly impact the performance of STs in IT mode. Besides, if the available energy cannot support the power control to achieve the SR's sensitivity, the ST will not transmit. So an ST's transmit power using channel inversion power control is

$$P_{\rho} = \begin{cases} \rho d^{\alpha}, & \dfrac{E_H - E_C}{1/M} > \rho d^{\alpha}, \\ 0, & \dfrac{E_H - E_C}{1/M} \leq \rho d^{\alpha}, \end{cases} \tag{14}$$

which can be rewritten as

$$P_{\rho} = \begin{cases} \rho d^{\alpha}, & E_H > \dfrac{\rho d^{\alpha}}{M} + E_C, \\ 0, & E_H \leq \dfrac{\rho d^{\alpha}}{M} + E_C. \end{cases} \tag{15}$$

The probability that an ST transmits at power P_{ρ}, which takes circuit power constraint into account, is

$$p_{\rho} = \mathbb{P}\left[E_H \geq \frac{\rho d^{\alpha}}{M} + E_C\right] = G\left(\frac{\rho d^{\alpha}}{M} + E_C\right), \tag{16}$$

where $G(\cdot)$ is given in (8). For convenience, $E_H > \rho d^{\alpha}/M + E_C$ is termed *power constraint with sensitivity* and p_{ρ} is termed *sensitivity satisfaction probability*. Since STs are independent from each other, working STs in IT mode adopting the power control form an HPPP Φ_{ρ} with intensity $\lambda_{\rho} = p_{\rho}\widetilde{\lambda}_{\text{it}} = p_{\rho}\lambda_{\text{ST}}/M$. Any working ST will transmit at power P_{ρ} and the remaining energy is ignored.

In the following, for convenience, when we analyze STs and PRs under power control, we still use notations which exist in normal settings, but with a slight difference when the notations involve STs in IT mode. For example, I_{it} under power control equals $\sum_{X_i \in \Phi_{\rho} \setminus \{X_0\}} P_{\rho} \| X_i - Z_0 \|^{-\alpha} g_i$.

3.2. Energy Storage and Reusing. As described above, an ST has a probability to get enough energy for transmitting in IT mode. If it does not get enough, in our previous settings, the unused energy is ignored and cannot be used in other time slots. Here we consider the setting that the energy can be stored, for a potential reusing. And we assume an ST has an energy storage component with capacity E_M. Besides, energy storage follows channel inversion power control, and the remaining energy when an ST can perform active transmission is also stored.

If the energy demand for active transmission is E_D, herein $E_D = \rho d^{\alpha}/M + E_C$, where E_C is the circuit power consumption, the stored energy in a time slot is

$$E_S = \begin{cases} E_H - E_D, & E_H > E_D, \\ E_H, & E_H \leq E_D. \end{cases} \tag{17}$$

Note that we assume an ST can detect whether the harvested energy is enough for active transmission before trying to transmit. If not enough, the ST will not work and cost no energy. Besides, the energy consumption for detection is ignored, so the harvest energy is E_H and we do not consider the case that $E_H < E_C$. From (8) we know the sensitivity satisfaction probability is $G(E_D)$; hence the expectation of stored energy is

$$\begin{aligned} \overline{E}_S &= \mathbf{E}\left[E_S\right] \\ &= G\left(E_D\right) \cdot \left(\mathbf{E}\left[E_H\right] - E_D\right) + \left(1 - G\left(E_D\right)\right) \cdot \mathbf{E}\left[E_H\right] \\ &= \mathbf{E}\left[E_H\right] - G\left(E_D\right) \cdot E_D. \end{aligned} \tag{18}$$

For ease of analysis, we assume once an ST has stored enough energy for active transmission before a time slot, it will use that energy in the slot. But the unused part and harvested energy in that slot are ignored. Therefore, the expectation of stored energy after $N_S = \lceil E_D/\overline{E}_S \rceil$ time slots is enough for another active transmission. So in the next time slot, an ST certainly has enough energy for active transmission, and the sensitivity satisfaction probability of the $N_S + 1$ slots increases to $(N_S G(E_D) + 1)/(N_S + 1)$. For simplicity we consider only the next time slot, so the increase of sensitivity satisfaction probability is

$$\begin{aligned} p_{\rho}^{\Delta} &= \left(\frac{N_S G\left(E_D\right) + 1}{N_S + 1} - G\left(E_D\right)\right)\left(1 - G\left(E_D\right)\right) \\ &= \frac{\left(G\left(E_D\right) - 1\right)^2}{N_S + 1}, \end{aligned} \tag{19}$$

where $1 - G(E_D)$ is the dissatisfaction probability, and this part means the improvement works only when harvested energy is not enough.

Although the reusing mechanism of stored energy is rough, it provides a view of reusing stored energy and increases the chance of active transmission.

Some point processes (p.p.) described in the paper, along with their descriptions, intensities (inten.), and values are listed in Table 1 to provide a clear view.

4. Coverage Probability and Achievable Rate

We analyze the coverage probabilities and average achievable rates of an SR in different communication modes and a PR, by using Shannon formula. The average rate is

$$\mathbf{E}\left[\log_2\left(1 + \text{SINR}\right)\right] = \mathbf{E}\frac{\left[\ln\left(1 + \text{SINR}\right)\right]}{\ln\left(2\right)}. \tag{20}$$

Besides, since SINR ≥ 0, it is easy to derive

$$\mathbf{E}\left[\ln\left(1 + \text{SINR}\right)\right] = \int_0^{\infty} \frac{1}{1+T} \mathbb{P}\left[\text{SINR} > T\right] \mathrm{d}T, \tag{21}$$

where T is the SINR threshold. So in the following, we will derive the coverage probability of the typical SR or PR in form

$$\mathbb{P}\left[\text{SINR} > T\right] = \mathbb{P}\left[\frac{S}{I + W} > T\right], \tag{22}$$

Table 1: Some point processes and their descriptions.

p.p.	Description	Inten.	Value
Φ_U	Primary users in a generic channel	λ_U	λ
Φ_{ST}	STs in a generic channel	λ_{ST}	$p_{\text{ch}}\lambda$
Φ_{eh}	STs in EH mode	λ_{eh}	$(D_E/M)\lambda_{\text{ST}}$
Φ_{bc}	STs in BC mode	λ_{bc}	$(D_B/M)\lambda_{\text{ST}}$
Φ_{bs}	Busy MBSs	λ_{bs}	$(1-1/M)\lambda$
$\widetilde{\Phi}_{\text{it}}$	STs in IT mode	$\widetilde{\lambda}_{\text{it}}$	λ_{ST}/M
Φ_{it}	Working STs in IT mode	λ_{it}	$p_{\text{sat}}\widetilde{\lambda}_{\text{it}}$
Φ_ρ	Working STs (power control)	λ_ρ	$p_\rho\widetilde{\lambda}_{\text{it}}$

where S is the desired signal, I is the interference, and W is the noise. After deriving the coverage probabilities, average rates can be easily obtained.

Firstly, we show some properties of the derivation processes which will be used for the following analysis and theorems.

Property 1. If the pdf of distance r from an MBS to an ST is $f_{\geq R_m}(r)$ in (2), the following expectation of r can be derived easily:

$$\mathbf{E}\left[r^{-2}\right] = \int_{r\geq R_m}^{R_M} r^{-2}\frac{2r}{R_M^2 - R_m^2}\mathrm{d}r = \frac{2\ln\left(R_M/R_m\right)}{R_M^2 - R_m^2}. \quad (23)$$

Property 2. If fading $h \sim \exp(\mu_h)$, the following expectation of h can be derived easily:

$$\mathbf{E}\left[h^{2/\alpha}\right] = \int_0^\infty \mu_h e^{-\mu_h h} h^{2/\alpha}\mathrm{d}h = \mu_h^{-2/\alpha}\Gamma\left(\frac{2}{\alpha}+1\right), \quad (24)$$

where α is the path-loss exponent and $\Gamma(z) = \int_0^\infty t^{z-1}e^{-t}\mathrm{d}t$ is the Gamma function.

Property 3. If y is a random variable, the following integral of y can be represented in nonintegral form:

$$K(\alpha) = \int_0^\infty \frac{y}{1+y^\alpha}\mathrm{d}y = \frac{\pi}{\alpha\sin\left(2\pi/\alpha\right)}, \quad (25)$$

where α is the path-loss exponent. Be similar to [26], we denoted the result in (25) as $K(\alpha)$ with some differences.

Property 4. Given the Laplace transform $\mathscr{L}_X(s)$ of a continuous random variable X, the pdf $f_X(x)$ of X can be recovered by inverse Laplace transform as [21]

$$f_X(x) = \mathscr{L}^{-1}\left\{\mathscr{L}_X(s)\right\}(x). \quad (26)$$

Note that, in this paper, we focus on a generic channel, a typical primary receiver, and a typical secondary receiver. Unless otherwise stated, the following analyzed coverage probabilities and average rates are analyzed under the setting that the receivers exist already.

4.1. Coverage Probability of an SR in BC Mode. Here we analyze the coverage probability of the typical secondary receiver working in backscatter mode; that is, its secondary transmitter backscatters signals for data transmission. The desired signal power is given in (4) and the interference is analyzed in Section 2.4.

Theorem 5. *The coverage probability of an SR in BC mode located at the origin is*

$$p_c^{bc} = \int_{r\geq R_m}^{R_M}\int_{q>0}^{\infty}\mu_q\exp\left(A_{bc} - B_{bc}C\right)\mathrm{d}q f_{\geq R_m}(r)\,\mathrm{d}r, \quad (27)$$

where

$$\begin{aligned} A_{bc} &= -\mu_q q - \frac{\mu_h}{\beta\eta_b q}TWd^\alpha r^\alpha, \\ B_{bc} &= \lambda_{bc}\left(\frac{\mu_h T}{\mu_g q}\right)^{2/\alpha} d^2, \\ C &= 2\pi r^2\mathbf{E}\left[R^{-2}\right]\mathbf{E}\left[h^{2/\alpha}\right]K(\alpha), \end{aligned} \quad (28)$$

and $\mathbf{E}[R^{-2}]$, $\mathbf{E}[h^{2/\alpha}]$, *and* $K(\alpha)$ *are given in (23), (24), and (25), respectively, where R is the distance from a generic interfering ST to its MBS having the same pdf given in (2).*

Proof. See Appendix. □

4.2. Coverage Probability of an SR in IT Mode. Here we analyze the coverage probability of the typical secondary receiver working in information transmission mode, that is, receiving signals transmitted by its secondary transmitter. The desired signal power is given in (11) and the interference is analyzed in Section 2.4.

Note that the typical ST in IT mode also has a probability of satisfying circuit power constraint, so the average coverage probability of the typical SR is

$$\overline{p}_c^{\text{it}} = \begin{cases} \mathbb{P}\left[\text{SINR}_{\text{it}} > T\right], & E_H \geq E_C, \\ 0, & E_H < E_C, \end{cases} \quad (29)$$

which can be further written as

$$\overline{p}_c^{\text{it}} = p_{\text{sat}}\mathbb{P}\left[\text{SINR}_{\text{it}} > T\right]. \quad (30)$$

Since p_{sat} has been analyzed, in the following, we mainly derive $p_c^{\text{it}} = \mathbb{P}[\text{SINR}_{\text{it}} > T]$ under the assumption that the typical ST satisfies the circuit power constraint, and *coverage probability* refers to p_c^{it} for convenience.

Theorem 6. *The coverage probability of an SR in IT mode located at the origin is*

$$p_c^{\mathrm{it}} = \int_{r\geq R_m}^{R_M} \int_{q>0}^{\infty} \mu_q \exp\left(A_{\mathrm{it}} - B_{\mathrm{it}}C - D_{\mathrm{it}}\right) \mathrm{d}q f_{\geq R_m}(r)\,\mathrm{d}r, \tag{31}$$

where

$$\begin{aligned} A_{\mathrm{it}} &= -\mu_q q - \frac{\mu_h TW}{\xi D_{\mathrm{eb}} q} d^{\alpha} r^{\alpha}, \\ B_{\mathrm{it}} &= \lambda_{\mathrm{it}} \left(\frac{\mu_h T}{\mu_g q}\right)^{2/\alpha} d^2, \\ D_{\mathrm{it}} &= 2\pi\lambda_{\mathrm{bs}} \left(\frac{\mu_h T}{\mu_g \xi D_{\mathrm{eb}} q}\right)^{2/\alpha} d^2 r^2 K(\alpha), \end{aligned} \tag{32}$$

and C is given in (28).

Proof. See Appendix. □

4.3. Coverage Probability of a PR. Here we analyze the coverage probability of the typical primary receiver with regard to interference from STs in IT mode. The desired signal comes from its MBS, and the interference is analyzed in Section 2.4.

Theorem 7. *The coverage probability of a PR located at the origin is*

$$p_c^{pr} = \int_{r>0}^{\infty} \exp\left(A_{pr} - B_{pr}C - D_{pr}\right) f(r)\,\mathrm{d}r, \tag{33}$$

where

$$\begin{aligned} A_{pr} &= -\mu_h TW r^{\alpha}, \\ B_{pr} &= \lambda_{it} \left(\frac{\xi D_{eb} \mu_h T}{\mu_g}\right)^{2/\alpha}, \\ D_{pr} &= 2\pi\lambda_{bs} \left(\frac{\mu_h T}{\mu_g}\right)^{2/\alpha} r^2 \int_{(\mu_g/(\mu_h T))^{1/\alpha}}^{\infty} \frac{y}{1+y^{\alpha}} \mathrm{d}y, \end{aligned} \tag{34}$$

and C is given in (28).

Proof. See Appendix. □

4.4. Coverage Probability of a PR without Interference from STs. Here we analyze the coverage probability of the typical primary receiver without interference from STs in IT mode. The desired signal still comes from the MBS and the primary receiver suffers only interference from other MBSs.

Theorem 8. *The coverage probability of a PR considering no interference from STs is*

$$p_c^{pr'} = \int_{r>0}^{\infty} \exp\left(A_{pr} - D_{pr}\right) f(r)\,\mathrm{d}r, \tag{35}$$

where A_{pr} and D_{pr} are given in (34).

Proof. See Appendix. □

4.5. Coverage Probability of an SR in IT Mode under Power Control. Here we analyze the coverage probability of the typical secondary receiver working in information transmission mode and adopting power control. The main differences are the transmit power of STs and their constraint satisfaction probability from p_{sat} to p_ρ.

Similarly to Section 4.2, coverage probability averaged over constraint satisfaction probability is

$$\overline{p}_{c,\rho}^{\mathrm{it}} = p_\rho \mathbb{P}\left[\mathrm{SINR}_{\mathrm{it}}^{\rho} > T\right], \tag{36}$$

and in the following, *coverage probability* refers to $p_{c,\rho}^{\mathrm{it}} = \mathbb{P}[\mathrm{SINR}_{\mathrm{it}}^{\rho} > T]$ under the assumption that the typical ST satisfies the power constraint with sensitivity.

Theorem 9. *The coverage probability of an SR in IT mode under power control is*

$$p_{c,\rho}^{it} = \exp\left(A_{it}^{\rho} - \lambda_\rho D_{it}^{\rho} - \lambda_{bs} P_\rho^{-2/\alpha} D_{it}^{\rho}\right), \tag{37}$$

where

$$\begin{aligned} A_{it}^{\rho} &= -\frac{\mu_q TW}{P_\rho} d^{\alpha}, \\ D_{it}^{\rho} &= 2\pi \left(\frac{\mu_q T}{\mu_g}\right)^{2/\alpha} d^2 K(\alpha). \end{aligned} \tag{38}$$

Proof. See Appendix. □

4.6. Coverage Probability of a PR under Power Control

Theorem 10. *The coverage probability of a PR suffering interference from STs in IT mode under power control is*

$$p_{c,\rho}^{pr} = \int_{r>0}^{\infty} \exp\left(A_{pr} - B_{pr}^{\rho} - D_{pr}\right) f(r)\,\mathrm{d}r, \tag{39}$$

where A_{pr}, D_{pr} are given in (34), and

$$B_{pr}^{\rho} = 2\pi\lambda_\rho \left(\frac{\mu_h T}{\mu_g}\right)^{2/\alpha} r^2 P_\rho^{2/\alpha} K(\alpha). \tag{40}$$

Proof. See Appendix. □

5. Numerical Results

We evaluate our analytical results by simulations. The simulation region is a square with side length of 10 km. The simulation results are obtained by averaging over 1000 runs. Unless otherwise stated, parameter values are listed in Table 2. To generate uniformly distributed points in an annular region, we use a native method of generating a random point within a circle with radius R_M, and if the random value is smaller than the inner radius R_m, the point will be generated repeatedly until it is in the annular region. A mathematical method is to use *inverse transform sampling*.

Table 2: Parameter value list.

Parameter	Value
Inner radius of annular regions R_m	5
Constant distance from an SR to its ST d	10
MBS density λ	5/km^2
Poisson distribution parameter Λ	3
Number of channels N_{ch}	4
Minislot number M	7
BC minislot number D_B	3 (i.e., $D_E = 3$)
Path-loss exponent α	4
Fading parameters μ_h, μ_g, μ_q	1
Noise W	−90 dBm
EH efficiency η	0.6
BC portion β	0.3
BC efficiency η_b	0.6
IT portion ξ	0.5
Circuit energy consumption E_C	−30 dBm
SR's sensitivity in IT mode	−60 dBm

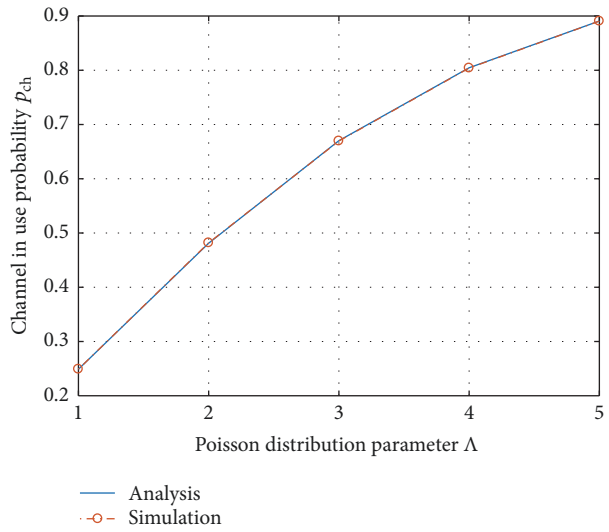

Figure 4: Channel in use probability versus Poisson distribution parameter (i.e., average number of STs clusters around an MBS).

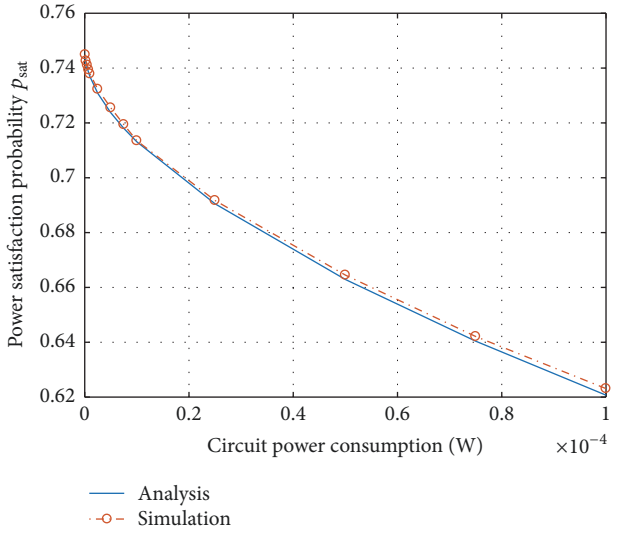

Figure 5: Power satisfaction probability of an ST.

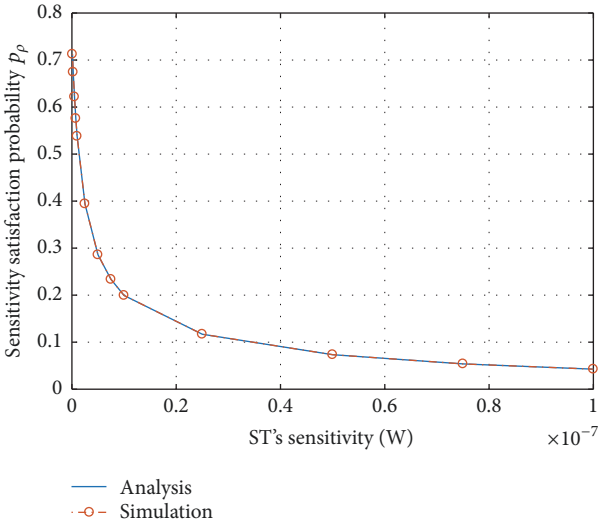

Figure 6: Sensitivity satisfaction probabilities of an ST under power control.

5.1. Channel in Use Probability. Figure 4 shows the channel in use probability p_{ch} given in (3). The simulation of channel selection is performed by random selection from all possible combinations. STs clustering around an MBS select idle channels using the method in Section 2.2; that is, they randomly select idle channels. We focus on the typical channel (numbered 1) and count how many typical channels are selected by STs clustering around all MBSs. The analytical and simulation curves overlap since the channel selection is simple, and the results are almost identical.

5.2. Power Satisfaction Probability and Sensitivity Satisfaction Probability. Figure 5 shows the power satisfaction probability p_{sat} given in (10), of an ST. As circuit power consumption E_C increases from −40 dBm (0.1 μW) to −10 dBm (0.1 mW), the probability decreases, but not much. The reason is that a larger E_C makes STs closer to MBSs, and STs then can harvest more energy to support a high satisfaction probability.

Figure 6 shows the sensitivity satisfaction probability p_ρ given in (16), of an ST under power control. As SRs' sensitivity ρ increases from −70 dBm to −50 dBm, p_ρ decreases sharply. The reason is that ρ does not change R_M, but requires more energy. And when ρ decreases further, the probability is already very low, so the change of satisfaction probability is small. The difference between these two figures also reveals the importance of R_M. Moreover, p_ρ is affected by circuit power constraint as well, which further affects the energy demand to transmit at P_ρ.

5.3. Coverage Probabilities. Figure 7 shows the analytical and simulated coverage probabilities of an ST in BC mode, IT

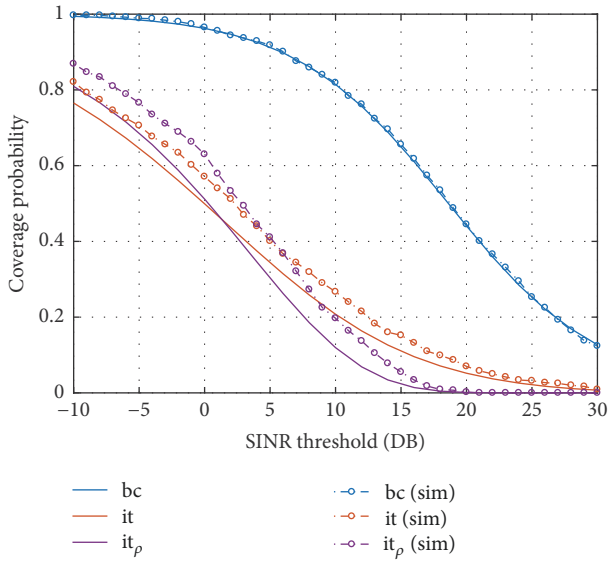

FIGURE 7: Analytical coverage probability of an ST in BC mode (bc), IT mode (it), and IT mode under power control (it$_\rho$).

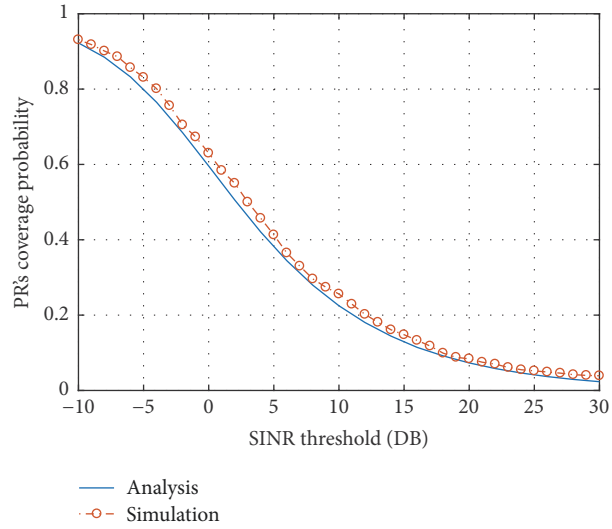

FIGURE 8: Analytical and simulated coverage probabilities of a PR.

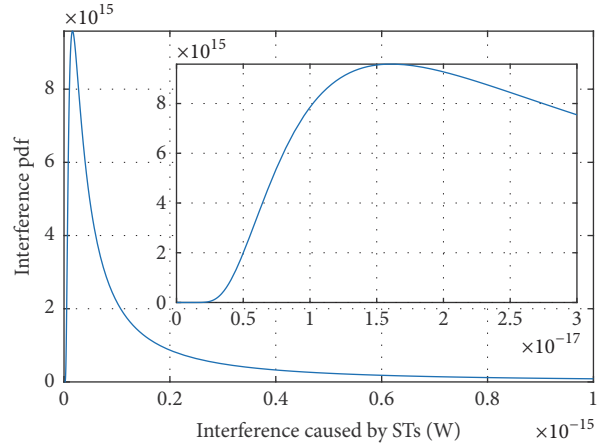

FIGURE 9: Analytical distribution of interference caused by STs in IT mode.

mode, and IT mode under power control. Since distance from an ST to its MBS and distance from an SR to its ST are both very short, signals decay not much. Besides, as described in Section 2.4, transmitted signals from MBSs and STs in IT mode make no interference to an SR in BC mode, so coverage probability of BC mode is much higher, while coverage probability of IT mode (under power control) is lower. Moreover, there is an intersection of curves of probabilities of IT mode and IT mode under power control. This happens since an SR in normal IT mode receives varied-power signals related to the ST's harvested energy. This means an ST may transmit at a high power, resulting in a high SINR, and may transmit at a low power, resulting in a low SINR. So the SINRs of SRs in normal IT mode range widely. On the other hand, an SR in IT mode under power control always receives constant-power (equals its sensitivity) signals from its ST, if fading is not considered. This means, there are few SRs having (extremely) low SINRs or high SINRs, which makes the curve shrink horizontally.

Note that these probabilities are not averaged over p_{sat} or p_ρ; that is, we assume the typical ST has already satisfied the constraints.

Figure 8 shows the analytical and simulated coverage probabilities of a PR. The probabilities of a PR interfered or not by STs in IT mode change too little to be observed, so the figure shows that only two curves represent analytical and simulated results. Since an ST transmits by using harvested energy, the transmit power is relatively lower to the power of MBSs. Besides, only STs whose MBSs are idle can transmit, and the idle ratio is low (1/7 in our settings), so the number of interfering STs to a PR is small. These are the two main reasons why STs' interference to a PR is so low. As for an SR in IT mode, since it is very close to its ST, it still gets high SINR even when the ST transmits at low power.

5.4. Distributions of Interference Caused by STs in IT Mode and under Power Control. As interference caused by STs in IT mode (and under power control) to a PR has quite limited effect on the PR's SINR, here we give the distributions of interference caused by STs. Following (26) in Property 4, (B.3) in Appendix, and (E.3) in Appendix, the analytical interference distributions caused by STs in IT mode and STs under power control are drawn in Figures 9 and 10, respectively.

5.5. Effect of Minislots Assignment on Coverage Probabilities. The different assignments of minislots, that is, different D_B and D_E, result into different numbers of STs in backscatter mode and energy harvesting mode, that is, intensities λ_{bc} and λ_{eh} of Φ_{bc} and Φ_{eh}, respectively. The intensity λ_{bc} does not affect backscatter power of an ST, because backscattering is instantaneous. But λ_{bc} affects interference power since it changes number of STs in backscatter mode. However, as described in previous subsection, SINR of an SR in BC mode is much higher, which means change of interference power

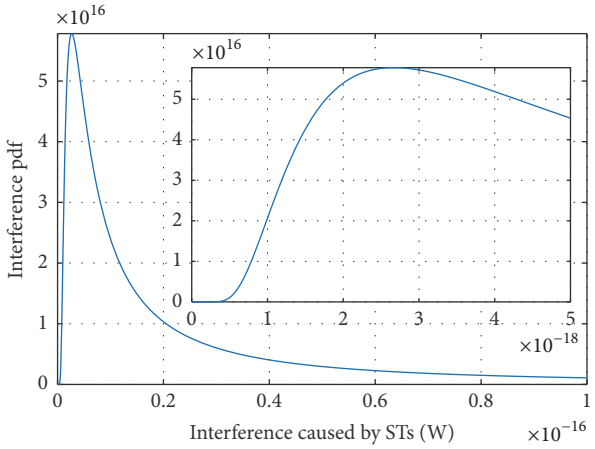

FIGURE 10: Analytical distribution of interference caused by STs in IT mode (under power control).

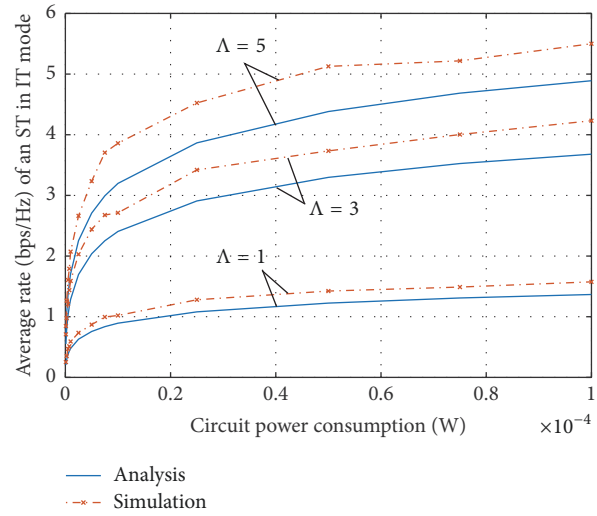

FIGURE 11: Average rates of an ST in IT mode versus circuit power consumption.

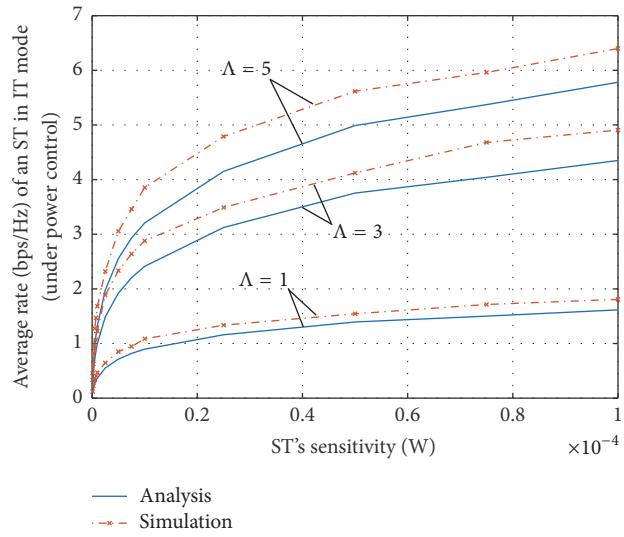

FIGURE 12: Average rates of an ST in IT mode under power control versus sensitivity.

makes little effect on the SINR, where noise W affects. So in both analytical and simulated results, when D_B changes from 1 to 5, p_c^{bc} varies quite little (less than 3%) when 5 dB is selected as the SINR threshold.

As for coverage probabilities of an SR in other modes, they change quite little, too (less than 1% and 4% in analytical and simulated results, resp.). The reason is that when D_B decreases, all STs harvest more energy (on average), so their transmit powers increase together. On the other hand, since we assume each MBS turns into idle in only one minislot, the minislots assignment does not affect number of STs in IT mode. Therefore, D_B makes little change on their SINRs. As for PR, since STs' impact of it is very limited as shown in the previous subsection, its SINR changes little (less than 1% and 3% in analytical and simulated results, resp.) when D_B varies.

5.6. Coverage Probabilities When Channels Are Fully Used. When considering special case *fully used channels*, $p_{\text{ch}} = 1$ holds and other settings remained. The analytical and simulated results of coverage probabilities in this case are very close to the above probabilities under normal settings. The analytical average changes over different SINR thresholds are 0.11%, 0.01%, 0.01%, 0%, 0%, and 0.01% corresponding to BC mode, IT mode, IT mode under power control, a PR, a PR without STs, and a PR (STs under power control), respectively. And the simulated average changes are 0.90%, 1.81%, 0.83%, 0.83%, 0.47%, and 0.83%, respectively. So when $N_{\text{ch}} = 4$ and Λ changes from 3 to a high enough value, the coverage probabilities change little.

5.7. Average Rates of STs in IT Mode. Figure 11 shows average rates of an ST in IT mode versus circuit power consumption E_C, with different Λ. As E_C increases, the rate becomes higher, too. This reason is that E_C affects R_M given in (7). A smaller E_C means a smaller R_M since STs have to be distributed closer to MBSs to get enough energy. However, since we assume a portion of the harvested energy can be used to perform information transmission, the power of the desired signal increases as well, resulting in a higher rate. Figure 12 shows average rates of an ST in IT mode under power control versus SRs' sensitivity ρ, with different Λ. As ρ increases, an SR receives a higher SINR because the desired signal is stronger, and there are less interfering STs.

Note that the rates are averaged over p_{ch} which represents the utility ratio of a channel by STs. Besides, since it is observed that STs in IT mode have limited interference to PRs, rates of a PR are omitted.

5.8. Average Stored Energy and Reusing. A larger circuit power consumption E_C or SRs' sensitivity ρ makes energy demand E_D higher, $G(E_D)$ lower, R_M smaller, and E_H higher. So the impact on average stored energy in a time slot $\overline{E}_S$ cannot be observed directly from (18). Figures 13 and 14 show

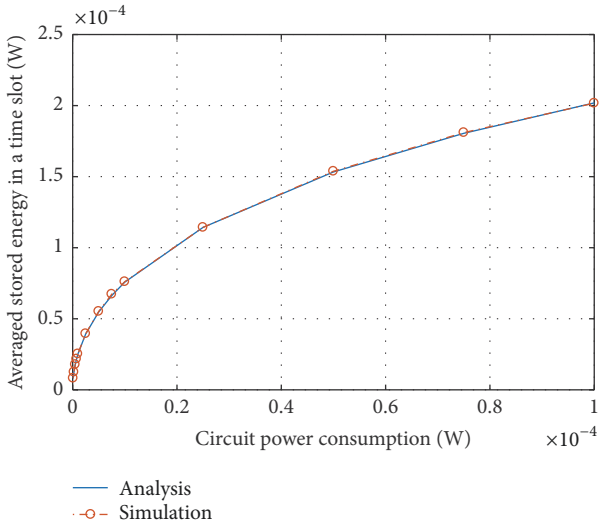

Figure 13: Average stored energy of an ST versus circuit power consumption.

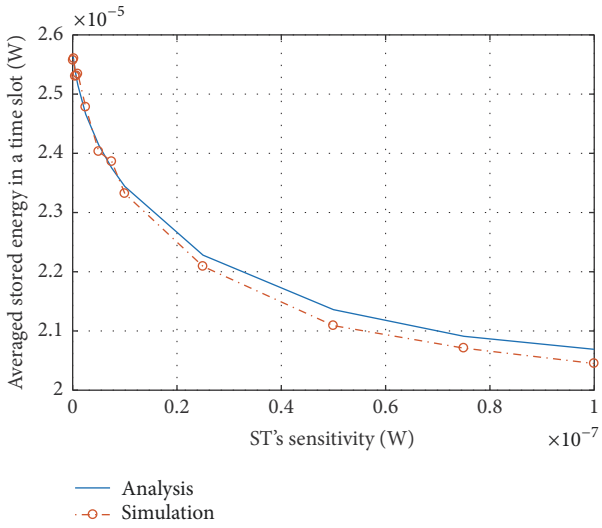

Figure 14: Average stored energy of an ST versus sensitivity.

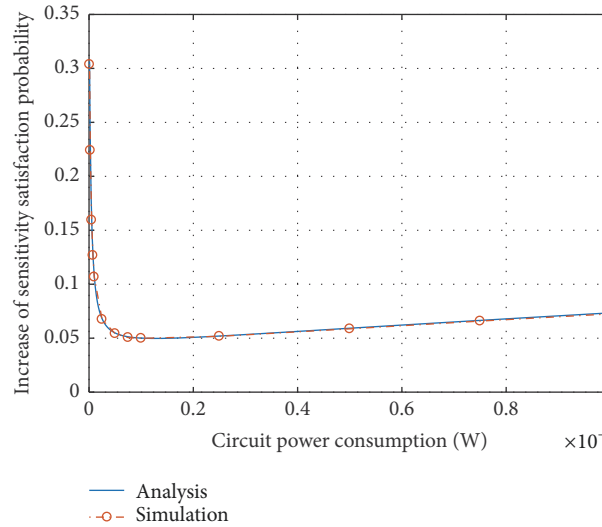

Figure 15: Average stored energy of an ST versus circuit power consumption.

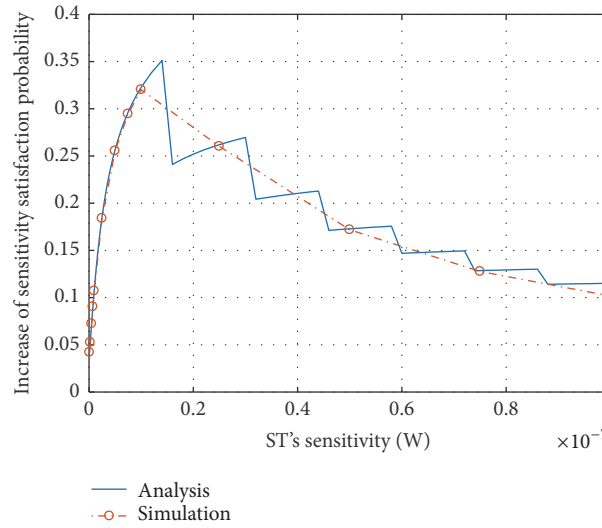

Figure 16: Average stored energy of an ST versus sensitivity.

the analytical and simulated results of $\overline{E}_S$ versus E_C and ρ, respectively.

Figures 15 and 16 show the sensitivity satisfaction probability increase p_ρ^Δ given in (19). These results are computed using (19), and the simulation data needed are obtained from simulations. Besides, analytical results are computed in small granularity (about 100 data points in both figures), while a spot of simulated data points is drawn in circles. Under our parameter settings, when E_C increases, p_ρ^Δ decreases sharply with a slow increase after that. But when ρ increases, p_ρ^Δ varies like a staircase function and decreases overall after the beginning increase. The staircase follows N_S which contains a ceiling function. Once the energy demand is large enough or averaged stored energy is less enough, N_S increases by 1, and the satisfaction probability drops down.

6. Conclusions

In this work, we have analyzed the performance of ambient backscatter communications in RF-powered cognitive radio networks based on stochastic geometry. Besides, we have applied channel inversion power control to active information of secondary users. After that, a simple energy storage and reusing mechanism has been designed and analyzed to improve utilization of harvested energy. Analytical results for constraint satisfaction probabilities and coverage probabilities of secondary users and of primary users considering both communication modes of secondary users have been obtained. Besides, average rates of secondary users have been obtained based on coverage probability. As for energy reusing, we have analyzed average stored energy during a time slot and the increase of constraint satisfaction

probability when power control is applied. The numerical results validate our theoretical analysis. Also, the results show performance improvement of secondary systems with only limited impact on the performance of primary systems. The analytical results and simulations demonstrate that integrating ambient backscatter communications into RF-powered cognitive radio network is a promising way to achieve energy and spectrum efficient wireless communications, which is suitable for certain Internet of things (IoT) applications.

Appendix

A. Proof of Theorem 5

By definition of coverage probability with SINR threshold T, we can start as

$$\begin{aligned} p_c^{\mathrm{bc}} &\triangleq \mathbb{P}\left[\mathrm{SINR}_{\mathrm{bc}} > T\right] = \mathbb{P}\left[\frac{P_{\mathrm{bc}} d^{-\alpha} q}{I_{\mathrm{bc}} + W} > T\right] \\ &= \mathbb{P}\left[\frac{\beta\eta_b r^{-\alpha} h d^{-\alpha} q}{I_{\mathrm{bc}} + W} > T\right] = \int_{r\geq R_m}^{R_M} \int_{q>0}^{\infty} \mu_q e^{-\mu_q q} \\ &\cdot \mathbb{P}\left[h > \frac{1}{\beta\eta_b q} T\left(I_{\mathrm{bc}} + W\right) d^{\alpha} r^{\alpha}\right] \mathrm{d}q \\ &\cdot f_{\geq R_m}(r)\, \mathrm{d}r, \end{aligned} \tag{A.1}$$

where P_{bc} is the backscatter power of the typical ST given in (4), r is the distance from the typical MBS to the typical ST, and d is the constant distance from the typical ST to the typical SR. The inner probability can be derived as

$$\begin{aligned} &\mathbb{P}\left[h > \frac{1}{\beta\eta_b q} T\left(I_{\mathrm{bc}} + W\right) d^{\alpha} r^{\alpha}\right] \\ &= \int_{i>0}^{\infty} \mathbb{P}\left[h > \frac{1}{\beta\eta_b q} T\left(I_{\mathrm{bc}} + W\right) d^{\alpha} r^{\alpha}\right] f_I(i)\, \mathrm{d}i \\ &= \exp\left(-\frac{\mu_h}{\beta\eta_b q} T W d^{\alpha} r^{\alpha}\right) \mathscr{L}_I\left(\frac{\mu_h}{\beta\eta_b q} T d^{\alpha} r^{\alpha}\right) \\ &= \exp\left(-sW\right) \mathscr{L}_{I_{\mathrm{bc}}}(s), \end{aligned} \tag{A.2}$$

where $s = (\mu_h/(\beta\eta_b q)) T d^{\alpha} r^{\alpha}$ and $\mathscr{L}_{I_{\mathrm{bc}}}(s)$ is the Laplace transform of I_{bc} and can be derived as

$$\begin{aligned} \mathscr{L}_{I_{\mathrm{bc}}}(s) &= \mathbf{E}\left[\exp\left(-sI_{\mathrm{bc}}\right)\right] \\ &= \mathbf{E}_{\Phi_{\mathrm{bc}}} \mathbf{E}_{P_{\mathrm{bc}_i}} \mathbf{E}_{g_i}\left[\exp\left(-s \sum_{X_i \in \Phi_{\mathrm{bc}} \setminus \{X_0\}} P_{\mathrm{bc}_i} \left\|X_i - Z_0\right\|^{-\alpha} g_i\right)\right] \\ &= \mathbf{E}_{\Phi_{\mathrm{bc}}} \prod_{X_i \in \Phi_{\mathrm{bc}} \setminus \{X_0\}} \mathbf{E}_{P_{\mathrm{bc}_i}} \mathbf{E}_{g_i}\left[\exp\left(-sP_{\mathrm{bc}_i} \left\|X_i - Z_0\right\|^{-\alpha} g_i\right)\right] \\ &= \exp\left(-2\pi\lambda_{\mathrm{bc}} \int_0^{\infty} \left(1 - \mathbf{E}_{P_{\mathrm{bc}}} \mathbf{E}_g\left[\exp\left(-sP_{\mathrm{bc}} x^{-\alpha} g\right)\right]\right) x\, \mathrm{d}x\right), \end{aligned} \tag{A.3}$$

where the last step follows from the probability generating functional of PPP [23]. The lower limit 0 follows from the fact that ST's positions are independent from each other, and SRs are in isotropic directions, so it could happen that another ST is close enough to an SR.

The inner expectation of g is

$$\begin{aligned} &\mathbf{E}_g\left[\exp\left(-sP_{\mathrm{bc}} x^{-\alpha} g\right)\right] \\ &= \int_0^{\infty} \mu_g e^{-\mu_g g} \exp\left(-sP_{\mathrm{bc}} x^{-\alpha} g\right) \mathrm{d}g \\ &= \int_0^{\infty} \mu_g \exp\left(-\left(\mu_g + sP_{\mathrm{bc}} x^{-\alpha}\right) g\right) \mathrm{d}g \\ &= \frac{1}{1 + \mu_g^{-1} sP_{\mathrm{bc}} x^{-\alpha}}. \end{aligned} \tag{A.4}$$

Plugging (A.4) into (A.3) gives

$$\begin{aligned} &\mathscr{L}_{I_{\mathrm{bc}}}(s) \\ &= \exp\left(-2\pi\lambda_{\mathrm{bc}} \int_0^{\infty} \mathbf{E}_{P_{\mathrm{bc}}}\left[\frac{1}{1 + 1/\left(\mu_g^{-1} sP_{\mathrm{bc}} x^{-\alpha}\right)}\right] \right. \\ &\left. \cdot\, x\, \mathrm{d}x\right). \end{aligned} \tag{A.5}$$

By changing the variable $x = (\mu_g^{-1} sP_{\mathrm{bc}})^{1/\alpha} y$, $\mathscr{L}_{I_{\mathrm{bc}}}(s)$ is further simplified as

$$\begin{aligned} &\mathscr{L}_{I_{\mathrm{bc}}}(s) \\ &= \exp\left(-2\pi\lambda_{\mathrm{bc}} \left(\mu_g^{-1} s\right)^{2/\alpha} \mathbf{E}\left[P_{\mathrm{bs}}^{2/\alpha}\right] \int_0^{\infty} \frac{y}{1 + y^{\alpha}} \mathrm{d}y\right), \end{aligned} \tag{A.6}$$

where

$$\mathbf{E}\left[P_{\mathrm{bs}}^{2/\alpha}\right] = \left(\beta\eta_b\right)^{2/\alpha} \mathbf{E}\left[R^{-2}\right] \mathbf{E}\left[h^{2/\alpha}\right], \tag{A.7}$$

where R is the distance from an interfering ST to its corresponding MBS with pdf $f_{\geq R_m}(R)$, which means $\mathbf{E}[R^{-2}]$ can be derived as (23). Besides, plugging s, $\mathbf{E}[P_{\mathrm{bs}}^{2/\alpha}]$, and (25) into $\mathscr{L}_{I_{\mathrm{bc}}}(s)$ gives

$$\begin{aligned} &\mathscr{L}_{I_{\mathrm{bc}}}(s) \\ &= \exp\left(-2\pi\lambda_{\mathrm{bc}} \left(\frac{\mu_h T}{\mu_g q}\right)^{2/\alpha} d^2 r^2 \mathbf{E}\left[R^{-2}\right] \mathbf{E}\left[h^{2/\alpha}\right] K(\alpha)\right). \end{aligned} \tag{A.8}$$

And plugging intermediate results into former equations will complete the proof.

Note that s here has no specific physical meaning, so for convenience, in other proofs, we still use the notation s with different values when we derive Laplace transforms.

B. Proof of Theorem 6

Here we show parts of the proof since it is similar to Appendix.

By definition of coverage probability,

$$p_c^{\mathrm{it}} \triangleq \mathbb{P}\left[\mathrm{SINR}_{\mathrm{it}} > T\right] = \mathbb{P}\left[\frac{P_{\mathrm{it}} d^{-\alpha} q}{I_{\mathrm{sum}} + W} > T\right]$$
$$= \mathbb{P}\left[\frac{\xi D_{\mathrm{eb}} r^{-\alpha} h d^{-\alpha} q}{I_{\mathrm{sum}} + W} > T\right] = \int_{r \geq R_m}^{R_M} \int_{q>0}^{\infty} \mu_q e^{-\mu_q q} \quad \text{(B.1)}$$
$$\cdot \mathbb{P}\left[h > \frac{T\left(I_{\mathrm{sum}} + W\right) d^{\alpha} r^{\alpha}}{\xi D_{\mathrm{eb}} q}\right] \mathrm{d}q f_{\geq R_m}(r)\, \mathrm{d}r,$$

where P_{it} is the transmit power of the typical ST in (11) and r and d are given in (A.1). By using the method in Appendix, it is easy to derive the inner probability as

$$\mathbb{P}\left[h > \frac{T\left(I_{\mathrm{sum}} + W\right) d^{\alpha} r^{\alpha}}{\xi D_{\mathrm{eb}} q}\right] = \exp\left(-sW\right) \mathscr{L}_{I_{\mathrm{sum}}}(s), \quad \text{(B.2)}$$

where $s = \mu_h T d^{\alpha} r^{\alpha} / (\xi D_{\mathrm{eb}} q)$. Since $I_{\mathrm{sum}} = I_{\mathrm{it}} + I_{\mathrm{bs}}$, we can get $\mathscr{L}_{I_{\mathrm{sum}}}(s) = \mathscr{L}_{I_{\mathrm{it}}}(s) \cdot \mathscr{L}_{I_{\mathrm{bs}}}(s)$. Continually following the steps in Appendix, we can derive the two Laplace transform components as

$$\mathscr{L}_{I_{\mathrm{it}}}(s)$$
$$= \mathbf{E}_{\Phi_{\mathrm{it}}} \mathbf{E}_{P_{\mathrm{it}_i}} \mathbf{E}_{g_i}\left[\exp\left(-s \sum_{X_i \in \Phi_{\mathrm{it}} \setminus \{X_0\}} P_{\mathrm{it}_i} \left\|X_i - Z_0\right\|^{-\alpha} g_i\right)\right] \quad \text{(B.3)}$$
$$= \exp\left(-2\pi\lambda_{\mathrm{it}} \left(\mu_g^{-1} s\right)^{2/\alpha} \mathbf{E}\left[P_{\mathrm{it}}^{2/\alpha}\right] K(\alpha)\right),$$

where

$$\mathbf{E}\left[P_{\mathrm{it}}^{2/\alpha}\right] = \left(\xi D_{\mathrm{eb}}\right)^{2/\alpha} \mathbf{E}\left[R^{-2}\right] \mathbf{E}\left[h^{2/\alpha}\right], \quad \text{(B.4)}$$

$$\mathscr{L}_{I_{\mathrm{bs}}}(s)$$
$$= \mathbf{E}_{\Phi_{\mathrm{bs}}} \mathbf{E}_{g_i}\left[\exp\left(-s \sum_{Y_i \in \Phi_{\mathrm{bs}} \setminus \{Y_0\}} \left\|Y_i - Z_0\right\|^{-\alpha} g_i\right)\right] \quad \text{(B.5)}$$
$$= \exp\left(-2\pi\lambda_{\mathrm{bs}} \left(\mu_g^{-1} s\right)^{2/\alpha} K(\alpha)\right).$$

Note that MBSs transmit at unit power, so there is no power notation before $\|Y_i - Z_0\|$. Finally, we can get the desired result by substituting intermediate results.

C. Proof of Theorem 7

Here we also give parts of the proof starting from definition of coverage probability:

$$p_c^{\mathrm{pr}} \triangleq \mathbb{P}\left[\mathrm{SINR}_{\mathrm{pr}} > T\right] = \mathbb{P}\left[\frac{r^{-\alpha} h}{I_{\mathrm{sum}} + W} > T\right]$$
$$= \int_{r>0}^{\infty} \mathbb{P}\left[h > T\left(\mathrm{I}_{\mathrm{sum}} + W\right) r^{\alpha}\right] f(r)\, \mathrm{d}r, \quad \text{(C.1)}$$

where r is the distance from the typical MBS to the typical PR, $f(r)$ is given in (1), and I_{sum} is given in (13). The inner probability is

$$\mathbb{P}\left[h > T\left(I_{\mathrm{sum}} + W\right) r^{\alpha}\right] = \exp\left(-sW\right) \mathscr{L}_{I_{\mathrm{sum}}}(s), \quad \text{(C.2)}$$

where $s = \mu_h T r^{\alpha}$. The first component of the Laplace transform $\mathscr{L}_{I_{\mathrm{it}}}(s)$ is the same as (B.3) except the specific value of s. The second component can be derived as

$$\mathscr{L}_{I_{\mathrm{bs}}}(s)$$
$$= \mathbf{E}_{\Phi_{\mathrm{bs}}} \mathbf{E}_{g_i}\left[\exp\left(-s \sum_{Y_i \in \Phi_{\mathrm{bs}} \setminus \{Y_0\}} \left\|Y_i - U_0\right\|^{-\alpha} g_i\right)\right]$$
$$= \exp\left(-2\pi\lambda_{\mathrm{bs}} \int_r^{\infty} \left(1 - \mathbf{E}_g\left[\exp\left(-sx^{-\alpha} g\right)\right]\right) x\, \mathrm{d}x\right) \quad \text{(C.3)}$$
$$= \exp\left(-2\pi\lambda_{\mathrm{bs}} \left(\mu_g^{-1} s\right)^{2/\alpha} \int_{r(\mu_g^{-1} s)^{-1/\alpha}}^{\infty} \frac{y}{1 + y^{\alpha}} \mathrm{d}y\right),$$

where the main difference is the lower limit r in the second equality, which follows from the fact that each PR is associated with its nearest MBS. The proof is similar to Appendix, so the remaining parts are omitted.

D. Proof of Theorem 8

Since the proof can be seen as parts of Appendix, we give only the definition of this coverage probability:

$$p_c^{\mathrm{pr}'} \triangleq \mathbb{P}\left[\mathrm{SINR}_{\mathrm{pr}'} > T\right] = \mathbb{P}\left[\frac{r^{-\alpha} h}{I_{\mathrm{bs}} + W} > T\right], \quad \text{(D.1)}$$

where I_{bs} is given in (13). The result follows from removing the part of interference of STs in Appendix and proof details are omitted.

E. Proof of Theorem 9

When adopting power control, the desired signal power and interfering power from other STs in IT mode both change, so these two components are the main differences when compared to p_c^{it} in Appendix.

By definition of coverage probability,

$$p_{c,\rho}^{\mathrm{it}} \triangleq \mathbb{P}\left[\mathrm{SINR}_{\mathrm{it}} > T\right] = \mathbb{P}\left[\frac{P_\rho d^{-\alpha} q}{I_{\mathrm{sum}} + W} > T\right]$$
$$= \mathbb{P}\left[q > \frac{T\left(I_{\mathrm{sum}} + W\right) d^{\alpha}}{P_\rho}\right], \quad \text{(E.1)}$$

where P_ρ is the transmit power of the typical ST and d is the constant distance from the typical ST to the typical SR. Different from Appendix, since the transmit power is constant, the derivation will be much simpler as the following:

$$\mathbb{P}\left[q > \frac{T\left(I_{\mathrm{sum}} + W\right) d^{\alpha}}{P_\rho}\right]$$
$$= \int_{i>0}^{\infty} \mathbb{P}\left[q > \frac{T\left(I_{\mathrm{sum}} + W\right) d^{\alpha}}{P_\rho}\right] f_I(i)\, \mathrm{d}i \quad \text{(E.2)}$$
$$= \exp\left(-sW\right) \mathscr{L}_{I_{\mathrm{sum}}}(s),$$

where $s = \mu_q T d^\alpha / P_\rho$. Similarly $\mathscr{L}_{I_{\text{sum}}}(s) = \mathscr{L}_{I_{\text{it}}^\rho}(s) \cdot \mathscr{L}_{I_{\text{bs}}}(s)$, and the two Laplace transform components can be derived as

$$\begin{aligned}
&\mathscr{L}_{I_{\text{it}}^\rho}(s) \\
&= \mathbf{E}_{\Phi_\rho} \mathbf{E}_{g_i} \left[\exp\left(-s \sum_{X_i \in \Phi_\rho \setminus \{X_0\}} P_\rho \left\| X_i - Z_0 \right\|^{-\alpha} g_i \right) \right] \quad \text{(E.3)} \\
&= \exp\left(-2\pi\lambda_\rho \left(\mu_g^{-1} s \right)^{2/\alpha} P_\rho^{2/\alpha} K(\alpha) \right),
\end{aligned}$$

and $\mathscr{L}_{I_{\text{bs}}}(s)$ is the same as (B.5) except the specific value of s. Substituting intermediate results will finish the proof.

F. Proof of Theorem 10

Since interfering power from other STs to a PR is the sole difference when STs adopt power control, only $\mathscr{L}_{I_{\text{it}}}(s)$ differs from that in Appendix. Moreover, it is the same as (E.3) except the specific value of s, and s is the same as that in Appendix. So we omit the proof details.

Notations

α: Path-loss exponent
β: Backscatter portion in BC mode
η, η_b: Signal to DC efficiency and backscatter efficiency
λ: Intensity of a point process
μ: Parameter of an exponential distribution (fading)
ξ: Available portion of harvested energy E_H
Φ: A Poisson point process
h: Fading of signal from an MBS to its ST or its PR
g: Fading of any interference signal
q: Fading of signal from an ST to its SR
p_c: Coverage probability
p_{ch}: Probability that a channel of a cell is used by an ST
p_{sat}: Circuit power constraint satisfaction probability
p_ρ: Probability that an ST transmits at power P_ρ
P, S, I, W: Transmit, desired signal, interference, and noise power
R_m, R_M: Inner and outer radii of the annular region
$\mathscr{L}_A(s)$: Laplace transform of r.v. A
$\mathbf{C}, c$: Channel set and a channel
M: Minislot number of a time slot
D_B, D_E: Backscatter and energy harvesting minislot number
E_H, E_C: Harvested energy and circuit power consumption
T: SINR Threshold
Y, U, X, Z: An MBS, a PR, an ST, and an SR (or their positions)
ρ: Sensitivity of an SR in IT mode
P_ρ: Transmit power considering power control
$\cdot_{\text{bs}}$ or $\cdot^{\text{bs}}$: Notations about busy MBSs
$\cdot_{\text{bc}}$ or $\cdot^{\text{bc}}$: Notations about STs in BC mode
$\cdot_{\text{it}}$ or $\cdot^{\text{it}}$: Notations about STs in IT mode or working STs
$\cdot_0$: The typical entities ($\cdot$ can be MBS, PR, ST, or SR).

Conflicts of Interest

The authors declare that there are no conflicts of interest regarding the publication of this paper.

Acknowledgments

This work was supported by Natural Science Foundation of China (61701230), Natural Science Foundation of Jiangsu Province (BK20170805, BK20160812), China Postdoctoral Science Foundation (2017M611806), Postdoctoral Science Foundation of Jiangsu Province (1701137A), research funding (2016-PYS/K-KY-J061), Foundation of Graduate Innovation Center in NUAA (KFJJ20171604), and the Fundamental Research Funds for the Central Universities.

References

[1] P. Zhang, M. Rostami, P. Hu, and D. Ganesan, "Enabling practical backscatter communication for on-body sensors," in *Proceedings of the 2016 ACM Conference on Special Interest Group on Data Communication, SIGCOMM 2016*, pp. 370–383, Brazil, August 2016.

[2] B. Kellogg, A. Parks, S. Gollakota, J. R. Smith, and D. Wetherall, "Wi-Fi backscatter: Internet connectivity for RF-powered devices," in *Proceedings of the 2014 ACM Conference on Special Interest Group on Data Communication, SIGCOMM 2014*, pp. 607–618, Chicago, Illinois, USA, August 2014.

[3] K. V. S. Rao, P. V. Nikitin, and S. F. Lam, "Antenna design for UHF RFID tags: a review and a practical application," *IEEE Transactions on Antennas and Propagation*, vol. 53, no. 12, pp. 3870–3876, 2005.

[4] V. Liu, A. Parks, V. Talla, S. Gollakota, D. Wetherall, and J. R. Smith, "Ambient backscatter: wireless communication out of thin air," in *Proceedings of the ACM Conference on SIGCOMM (SIGCOMM '13)*, pp. 39–50, Hong Kong, China, August 2013.

[5] X. Lu, P. Wang, D. Niyato, D. I. Kim, and Z. Han, "Wireless networks with RF energy harvesting: a contemporary survey," *IEEE Communications Surveys & Tutorials*, vol. 17, no. 2, pp. 757–789, 2015.

[6] S. Lee, R. Zhang, and K. Huang, "Opportunistic wireless energy harvesting in cognitive radio networks," *IEEE Transactions on Wireless Communications*, vol. 12, no. 9, pp. 4788–4799, 2013.

[7] V. Rakovic, D. Denkovski, Z. Hadzi-Velkov, and L. Gavrilovska, "Optimal time sharing in underlay cognitive radio systems with RF energy harvesting," in *Proceedings of the IEEE International Conference on Communications, ICC '15*, pp. 7689–7694, London, UK, June 2015.

[8] H. D. Thai, D. Niyato, P. Wang, D. I. Kim, and Z. Han, "The tradeoff analysis in RF-powered backscatter cognitive radio networks," in *Proceedings of the 59th IEEE Global Communications Conference, GLOBECOM 2016*, Washington, D.C., USA, December 2016.

[9] F. Akhtar, M. H. Rehmani, and M. Reisslein, "White space: definitional perspectives and their role in exploiting spectrum opportunities," *Telecommunications Policy*, vol. 40, no. 4, pp. 319–331, 2016.

[10] M. Monemi, M. Rasti, and E. Hossain, "Characterizing feasible interference region for underlay cognitive radio networks," in *Proceedings of the IEEE International Conference on Communications, ICC 2015*, pp. 7603–7608, London, UK, June 2015.

[11] M. Monemi, M. Rasti, and E. Hossain, "On Characterization of Feasible Interference Regions in Cognitive Radio Networks," *IEEE Transactions on Communications*, vol. 64, no. 2, pp. 511–524, 2016.

[12] Y. Saleem and M. H. Rehmani, "Primary radio user activity models for cognitive radio networks: a survey," *Journal of Network and Computer Applications*, vol. 43, pp. 1–16, 2014.

[13] Y. Chen and H.-S. Oh, "A survey of measurement-based spectrum occupancy modeling for cognitive radios," *IEEE Communications Surveys & Tutorials*, vol. 18, no. 1, pp. 848–859, 2016.

[14] M. Eskola, M. Matinmikko, J. Kalliovaara et al., "Spectrum occupancy measurements: A survey and use of interference maps," *IEEE Communications Surveys & Tutorials*, vol. 18, no. 4, pp. 2386–2414, 2016.

[15] X. Xing, T. Jing, W. Cheng, Y. Huo, and X. Cheng, "Spectrum prediction in cognitive radio networks," *IEEE Wireless Communications Magazine*, vol. 20, no. 2, pp. 90–96, 2013.

[16] X. Lu, D. Niyato, H. Jiang, D. I. Kim, Y. Xiao, and Z. Han, "Ambient Backscatter Assisted Wireless Powered Communications," *IEEE Wireless Communications Magazine*, pp. 2–9, 2018.

[17] D. T. Hoang, D. Niyato, P. Wang, and D. I. Kim, "Optimal time sharing in RF-powered backscatter cognitive radio networks," in *Proceedings of the 2017 IEEE International Conference on Communications, ICC 2017*, Paris, France, May 2017.

[18] S. H. Kim and D. I. Kim, "Hybrid Backscatter Communication for Wireless-Powered Heterogeneous Networks," *IEEE Transactions on Wireless Communications*, vol. 16, no. 10, pp. 6557–6570, 2017.

[19] K. Han and K. Huang, "Wirelessly Powered Backscatter Communication Networks: Modeling, Coverage, and Capacity," *IEEE Transactions on Wireless Communications*, vol. 16, no. 4, pp. 2548–2561, 2017.

[20] X. Lu, H. Jiang, D. Niyato, D. I. Kim, and P. Wang, "Analysis of Wireless-Powered Device-to-Device Communications with Ambient Backscattering," in *Proceedings of the 2017 IEEE 86th Vehicular Technology Conference (VTC-Fall)*, pp. 1–6, Toronto, ON, Canada, September 2017.

[21] X. Lu, H. Jiang, D. Niyato, D. I. Kim, and Z. Han, "Wireless-Powered Device-to-Device Communications with Ambient Backscattering: Performance Modeling and Analysis," *IEEE Transactions on Wireless Communications*, vol. 17, no. 3, pp. 1528–1544, 2018.

[22] M. Haenggi, "A geometric interpretation of fading in wireless networks: theory and applications," *Institute of Electrical and Electronics Engineers Transactions on Information Theory*, vol. 54, no. 12, pp. 5500–5510, 2008.

[23] J. G. Andrews, F. Baccelli, and R. K. Ganti, "A tractable approach to coverage and rate in cellular networks," *IEEE Transactions on Communications*, vol. 59, no. 11, pp. 3122–3134, 2011.

[24] X. Lin, J. G. Andrews, and A. Ghosh, "Spectrum sharing for device-to-device communication in cellular networks," *IEEE Transactions on Wireless Communications*, vol. 13, no. 12, pp. 6727–6740, 2014.

[25] Y. J. Chun, M. O. Hasna, and A. Ghrayeb, "Modeling heterogeneous cellular networks interference using poisson cluster processes," *IEEE Journal on Selected Areas in Communications*, vol. 33, no. 10, pp. 2182–2195, 2015.

[26] K. Zhu and E. Hossain, "Joint mode selection and spectrum partitioning for device-to-device communication: a dynamic stackelberg game," *IEEE Transactions on Wireless Communications*, vol. 14, no. 3, pp. 1406–1420, 2015.

[27] D. Stoyan, W. S. Kendall, and J. Mecke, *Stochastic geometry and its applications*, Wiley Series in Probability and Mathematical Statistics: Applied Probability and Statistics, John Wiley & Sons, Ltd., Chichester, New York, NY, USA, 1995.

[28] Y. L. Che, L. Duan, and R. Zhang, "Spatial Throughput Maximization of Wireless Powered Communication Networks," *IEEE Journal on Selected Areas in Communications*, vol. 33, no. 8, pp. 1534–1548, 2015.

[29] H. ElSawy, E. Hossain, and M.-S. Alouini, "Analytical modeling of mode selection and power control for underlay D2D communication in cellular networks," *IEEE Transactions on Communications*, vol. 62, no. 11, pp. 4147–4161, 2014.

[30] K. S. Ali, H. ElSawy, and M.-S. Alouini, "Modeling Cellular Networks with Full-Duplex D2D Communication: A Stochastic Geometry Approach," *IEEE Transactions on Communications*, vol. 64, no. 10, pp. 4409–4424, 2016.

[31] H. Ju and R. Zhang, "Throughput maximization in wireless powered communication networks," *IEEE Transactions on Wireless Communications*, vol. 13, no. 1, pp. 418–428, 2014.

[32] W. Liu, K. Huang, X. Zhou, and S. Durrani, "Time-Hopping Multiple-Access for Backscatter Interference Networks," in *Proceedings of the GLOBECOM 2017 - 2017 IEEE Global Communications Conference*, pp. 1–7, Singapore, December 2017.

[33] A. H. Sakr and E. Hossain, "Cognitive and energy harvesting-based D2D communication in cellular networks: stochastic geometry modeling and analysis," *IEEE Transactions on Communications*, vol. 63, no. 5, pp. 1867–1880, 2015.